# Trade-off between quantum and thermal fluctuations in mirror coatings yields improved sensitivity of gravitational-wave interferometers

N. V. Voronchev, S. L. Danilishin, and F. Ya. Khalili

Phys. Rev. D **86**, 122003 — Published 17 December 2012

DOI: 10.1103/PhysRevD.86.122003

# Trade-off between quantum and thermal fluctuations in mirror coatings yields improved sensitivity of gravitational-wave interferometers

N.V. Voronchev,[1,*] S.L. Danilishin,[2,†] and F.Ya. Khalili[1,‡]

[1] *Faculty of Physics, Moscow State University, Moscow 119991, Russia*
[2] *School of Physics, University of Western Australia, 35 Stirling Hwy, Crawley 6009, WA, Australia*

We propose a simple way to improve the sensitivity of laser gravitational-wave detectors and other high-precision laser interferometric position meters by means of reduction of the number of reflective coating layers of the core optics mirrors. This effects in the proportional decrease of the coating thermal noise, the most notorious among the interferometers technical noise sources. The price for this is the increased quantum noise, as well as high requirements for the pump laser power and, therefore, power at the beam splitter, the power recycling mirror, and the arm cavities input mirrors substrates. However, as far as these processes depend differently on the coating thickness, we demonstrate that a certain trade-off is possible. In the particular case of large-scale laser gravitational-wave detectors, this trade-off yields a 20 - 30% gain (for diverse gravitational wave signal types and interferometer configurations), provided that increased laser power (comparable with that planned for the third generation gravitational-wave detectors) becomes available and that it will be possible to mitigate the increased thermal effects caused by absorption in the beam splitter and input mirrors.

## I. INTRODUCTION

Among the multitude of noise sources limiting the sensitivity of contemporary laser gravitational-wave (GW) detectors (LIGO [1, 2], VIRGO [3, 4], GEO-600 [5, 6], and TAMA [7, 8]), the one, usually referred to as *quantum* noise and stemming from the quantum nature of light, stands apart from the rest of the noise sources, referred to as *technical* or *classical* ones. Quantum noise originates from quantum fluctuations of phase (shot noise) and intensity (radiation-pressure noise) of light circulating inside the interferometers, which obey Heisenberg's uncertainty relation [9] and therefore can not be reduced simultaneously. The latter group comprises various fluctuations of thermal, seismic and similar origin that can be, in principle, diminished either by cooling, or using better materials, more sophisticated seismic isolation *etc.* All the hitherto undertaken efforts towards the improvement of GW interferometers sensitivity went in two parallel but virtually independent streams. In many proposed methods of diverse technical noise sources mitigation [10–18], the authors assumed quantum noise of the interferometer as independent of the technical noise budget and thus did not take it into consideration. Independently, the researchers of the quantum noise proposed a plenty of sophisticated and witty ways for the quantum noise reduction [19–33] tacitly imply the technical noise sources being independent on the quantum fluctuations of light inside the interferometer.

However, the growing interest to the optimal configurations of future GW detectors, inspired by the recent achievements in reduction of technical noise in first-generation detectors and a proximity of the start of construction of the second generation ones, has brought the problem of simultaneous treatment of the two groups of noise sources to the fore [29, 30]. Indeed, the sensitivity of the current first generation detectors (for example, LIGO, which has already finished its life cycle) is limited mostly by seismic noise at lower frequencies (below $\sim 100\,\mathrm{Hz}$) and by the quantum shot noise at higher frequencies. In the next-generation detectors, such as Advanced LIGO [34–36], Advanced VIRGO [37], and LCGT [38], the technical noise will be reduced significantly by using much better seismic isolation and other technological advances. Along with this, the quantum shot noise will be suppressed by about one order of magnitude due to increased optical power and, very probably, by the injection of the quantum squeezed light into the interferometer, as it has been proposed first in [9] (this technology has been successfully tested experimentally in GEO-600 [39]). Yet the second generation detectors sensitivity remain bound by the mix of the technical and quantum noise: (i) shot noise at high frequencies, (ii) radiation-pressure noise at low frequencies, and (iii) coatings thermal noise in the best sensitivity medium frequencies band around 100 Hz (see Fig. 3 of the paper [35]).

In this article, we make a further step forward and consider quantum noise and coating thermal noise in conjunction. The importance of thermal fluctuations in core optics dielectric coatings was realised by the community several years ago [40]. All the hitherto proposed ways to reduce these fluctuations, were it based on broadening of laser beams [10, 11, 14, 16], or on using better coating materials [12], or on coating structure optimization [13, 15, 17], followed implicitly a common rule that the end mirrors (ETMs) of the interferometer should be as reflective as possible thus requiring the number of coating layers to be pretty large (ca. 40). But since the power spectral density of these fluctuation rises linearly with the number of coating layers, the improvement provided

* n.voronchev@physics.msu.ru
† shtefan.danilishin@uwa.edu.au
‡ khalili@phys.msu.ru

by these methods is rather modest.

Another apparent way to get rid of coating noise by getting rid of the (at least a part of) the coating itself was proposed even earlier. In [41], authors suggested to replace the end mirrors by coatingless corner reflectors, while in [42] the short anti-resonance-tuned Fabry-Pérot cavities have to play the role of ETMs. This method is planned currently for the Hannover 10-m prototype interferometer [43], devoted to development of practical methods of overcoming the SQL in optomechanical experiments.

Even more radical solution to use the pass-through Mach-Zehnder/Fabry-Pérot topology instead of the Michelson/Fabry-Pérot one was suggested in [44]. However, the implementation of these methods in the near future is improbable, for corner reflectors were shown to have high optical losses [45] and the latter two solutions require too radical modifications of the GW detector optical setup. In particular, the additional anti-resonance-tuned cavities are considered as one of the most hard to implement parts of the 10-m prototype interferometer, which should be avoided if possible [46].

The requirement for the ETMs of the standard Michelson/Fabry-Pérot scheme of high-precision interferometers (see Fig. 1) to have high reflectivity has rather strong logic behind. There are two obvious reasons in favour of it. First, in the power-recycled topology, the value of ETM power reflectivity $R_{\rm ETM}$ defines how much circulating power $I_c$ can be built up in the arm cavities, for a given value of the input laser power $I_0$:

$$I_c \le \frac{I_0}{2(1-R_{\rm ETM})}\,. \qquad (1)$$

Simple estimate based on the values of $I_0$ and $I_c$ planned for the Advanced LIGO yields $1-R_{\rm ETM} \lesssim 10^{-4}$. Second, a non-ideal reflectivity of the end mirrors means an injection of additional optical vacuum fluctuations into the arm cavities, that is, the increase of the quantum noise.

But if we ask ourselves a question whether this requirement always provides unconditionally optimal sensitivity, we claim that the answer will be 'no'. The circulating power issue can be solved either by using more powerful laser, or by using squeezed vacuum injection as it might be done in the Advanced LIGO [47].

Regarding the influence of the additional vacuum fields entering the arm cavities through the more transparent ETMs, it is evident, that in the scenario where the total noise budget, in the best sensitivity frequency band, is dominated by the mirrors coatings thermal noise, it is reasonable to reduce the number of coating layers of the end mirrors, increasing the quantum noise, but decreasing the coatings thermal noise.

Therefore, the number of layers of the core optics coatings should be included into the set of optical parameters, such as arm cavities bandwidth, the signal recycling mirror transmittance and the the signal recycling cavity detuning, over which the minimization of the sum noise of the interferometer is run.

In this paper, we perform this kind of optimization for the signal- and power-recycled Fabry-Pérot–Michelson interferometer (see Fig. 1), assuming its main parameters close to the ones planned for the Advanced LIGO. In the next section, we describe the variants of the advanced gravitation-wave detectors scheme which we optimize, the model of technical noise and quantum noise which we use, and the optimization procedure. In Sec. III, we discuss the results of optimization.

## II. OPTIMIZED CONFIGURATIONS AND THE OPTIMIZATION PROCEDURE

### A. Interferometer configurations

The following configurations are considered in this paper (see Fig. 1):

- Plain: the ordinary signal- and power-recycled interferometer, similar to the Advanced LIGO, with vacuum input (no squeezing).
- Squeezed: the same as the above, but with squeezed light injection into the dark port.
- Pre-filtering: the same as previous, but with frequency-dependent squeezing angle implemented by means of the additional input filter cavity.
- Post-filtering: the back action evading configuration with the additional output filter cavity and the squeezed light injection into the dark port.

The last two configurations, in a more sophisticated two-cavities form, were first proposed in paper [25]. Here we consider more simple cases with only one relatively short filter cavity. Estimates (see, *e.g*, [48]) show that in the presence of the technical noise, single filter cavity configurations provide almost the same sensitivity as the two-cavity ones, while being much less expensive in implementation. It was shown also in the paper [48] that the sensitivity of these *phase filtering* schemes is better than that of the *amplitude filtering* configuration [27, 31, 49]. Currently, it is these two schemes that are considered as the most probable variants for upgrading the Advanced LIGO.

For all these topologies, except for the post-filtering one, we assume a DC readout photodetection scheme which is planned for the Advanced LIGO interferometer. We limit ourselves to the simplest particular case of this scheme, namely, the one where the lengths of the arm cavities differ by a small *DC offset*, remaining identical in all other aspects. This particular case corresponds to a homodyne detection with the homodyne angle equal to $\pi/2$ (phase detection).

For the post-filtering topology, the DC readout can not be used for obvious reason. With a non-zero DC-component of the outgoing light present, any fluctuations

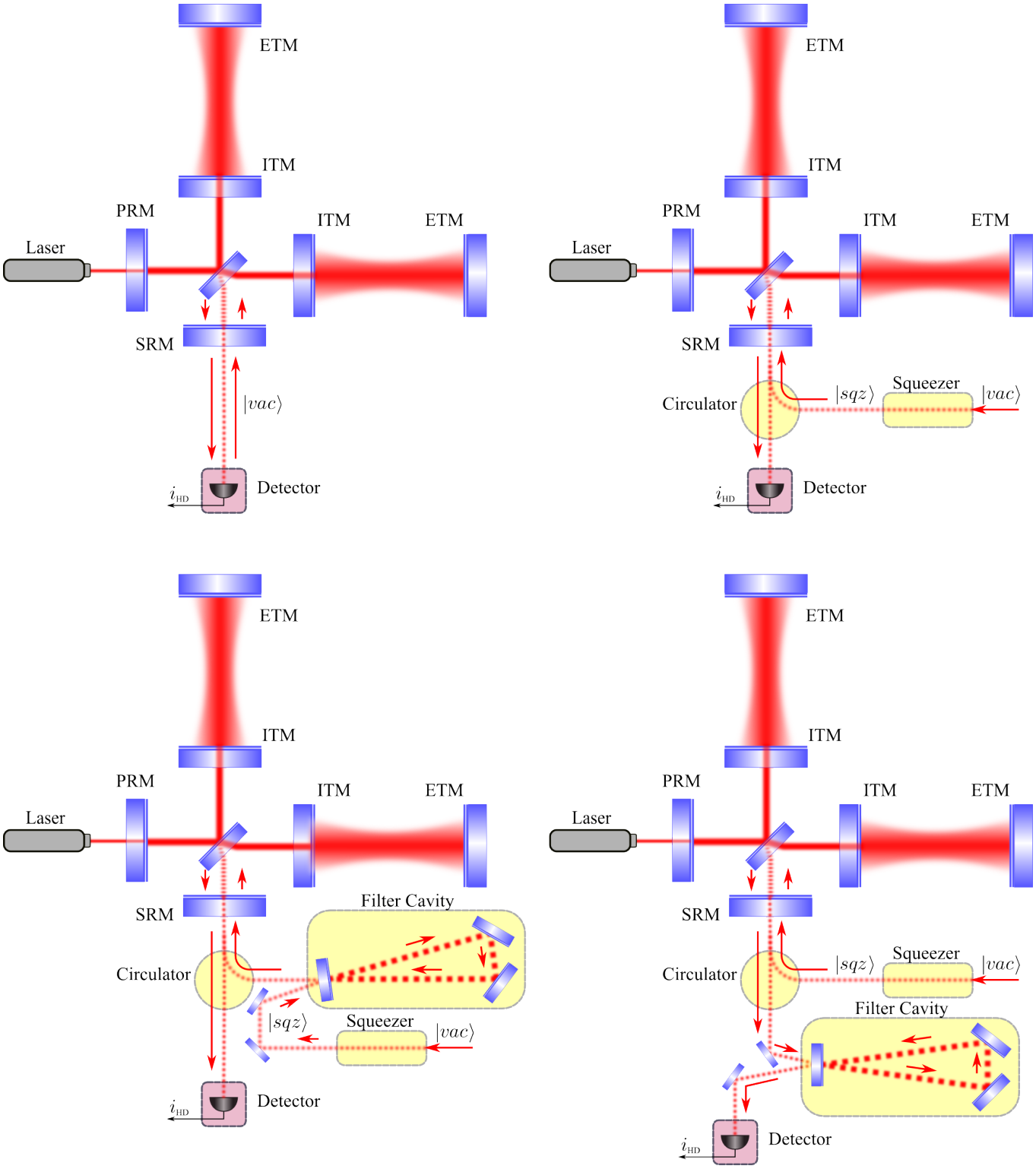


FIG. 1. The schemes of the advanced gravitation-wave detector being considered in this paper. Top left: the signal- and power-recycled interferometer similar to the one planned for Advanced LIGO [35] (referred to as "plain"). Top right: the configuration with frequency-independent squeezed light injection into the dark port (referred to as "squeezed"). Bottom left: the configuration with injection of frequency-dependent squeezed light created by means of the input filter cavity (referred to as "pre-filtering"). Bottom right: the back action evading configuration with the additional output filter cavity and the squeezed light injection into the dark port (referred to as "post-filtering").

TABLE I. The main parameters and their numerical values.

| Parameter | Value | Description |
|---|---|---|
| $\omega_p$ | $2\pi c/(1.064\,\mu\text{m})$ | Optical pump frequency |
| $M$ | 40 kg | Mirrors mass |
| $L$ | 4 km | Interferometer arms length |
| $I_0$ | $\leq 500$ W | Input optical power |
| $I_c$ | 200 kW or 840 kW | Circulating power in the arms |
| $I_{\rm abs}$ | $\leq 1$ W | Power absorption in the ITMs and in the beamsplitter. |
| $\eta$ | 0.9 | Photodetectors quantum efficiency |
| $l$ | 50 m | Filter cavity length |
| $A_f$ | 10 ppm | Filter cavity losses per bounce |

of the filter cavity mirrors positions would result in an additional phase noise in the output beam. Therefore, we consider a homodyne detection scheme with tunable homodyne angle for this topology.

Following the Advanced LIGO design, we assume that the power- and the signal-recycling mirror are used in the interferometer, as shown in Fig. 1. For those of the considered topologies which rely on the DC readout, we limit ourselves to two simple cases of *extreme signal-recycling* and *resonant-sideband-extraction*, which give the resonant-tuned interferometer, because for all other tunings, fluctuations of the signal recycling mirror position in presence of the outgoing DC power will lead to the additional phase noise. For the homodyne detection based post-filtering scheme, we consider the general *detuned signal recycling* case.

For the main parameters of the considered schemes, we assume the values close to the ones planned for the Advanced LIGO and its upgrades [35, 36], see Table I. We suppose, however, that the input power can be higher, up to 500 W, and for the circulating power, along with the "canonical" value of 840 kW, we consider the reduced one equal to 200 kW.

### B. Figures of merit

The common figure of merit for the gravitational wave detectors sensitivity is the signal-to-noise ratio integral (SNR) for some standard gravitational waves source:

$$\rho^2(N_{\rm ITM}, N_{\rm ETM}; \mathbf{p}) = \int_{\Omega_{\rm min}}^{\Omega_{\rm max}} \frac{|h(\Omega)|^2}{S^h(\Omega; N_{\rm ITM}, N_{\rm ETM}; \mathbf{p})} \frac{d\Omega}{2\pi}\,, \tag{2}$$

where $\Omega_{\rm min}$ and $\Omega_{\rm max}$ are the minimal and the maximal frequencies of the GW detector sensitivity band, which we assume to be equal to $2\pi\times 5$ Hz and $2\pi\times 5$ kHz, respectively; $h(\Omega)$ is the strain spectrum of the gravitational wave signal;

$$S^h(\Omega; N_{\rm ITM}, N_{\rm ETM}; \mathbf{p}) = S^h_{\rm quant}(\Omega; N_{\rm ITM}, N_{\rm ETM}; \mathbf{p}) + S^h_{\rm coat}(\Omega; N_{\rm ITM}, N_{\rm ETM}) + S^h_{\rm tech}(\Omega) \tag{3}$$

is the spectral density of the sum noise normalized as the equivalent gravitational wave strain variation; $S^h_{\rm quant}(\Omega; N_{\rm ITM}, N_{\rm ETM}; \mathbf{p})$ is the quantum noise spectral density which depends on the numbers $N_{\rm ITM}$ and $N_{\rm ETM}$ of the coating layers doublets of the input and the end mirrors, respectively, as well as on the vector $\mathbf{p}$ of other optical parameters of the interferometer (we specify this vector below); $S^h_{\rm coat}(\Omega; N_{\rm ITM}, N_{\rm ETM})$ is the mirrors coating thermal noise spectral density, which also depends on $N_{\rm ITM}$ and $N_{\rm ETM}$; and $S^h_{\rm tech}(\Omega)$ is the sum spectral density of the rest of technical noise sources.

For our optimization, we will use two standard types of the gravitational wave sources, (see, *e.g*, [50]). The first one is the GW signal from the inspiral stage of the binary neutron stars (BNS) collisions with

$$|h_{\rm BNS}(\Omega)|^2 = K_{\rm BNS}\times\begin{cases}\Omega^{-7/3}\,, & \Omega \leq 2\pi\times 1.5\,\text{kHz}\,,\\ 0\,, & \Omega > 2\pi\times 1.5\,\text{kHz}\,,\end{cases} \tag{4}$$

which accounts mostly for the low-frequency noise. The second one is the gravitational wave "bursts", with

$$|h_{\rm Burst}(\Omega)|^2 = \frac{K_{\rm Burst}}{\Omega}\,, \tag{5}$$

which requires more broadband sensitivity from the detector. Here $K_{\rm BNS}$ and $K_{\rm Burst}$ are some factors, depending on the astrophysical parameters of the signal source but not on the observation frequency $\Omega$ and the detector optical parameters.

Our treatment of the interferometer quantum noise is based on the works [25, 48, 51]. The corresponding explicit equations for the quantum noise spectral densities $S^h_{\rm quant}$ are too cumbersome to be shown here, especially for the filter cavities based configurations, and can be found in the Appendix.

In our calculation of the coating Brownian noise spectral density $S^h_{\rm coat}$, we follow the paper [17], which takes into account additional effects of light interference in the coating layers as well as the photoelastic effect. This method gives more precise correct estimate for the coating Brownian noise spectral density, which is smaller than the previous estimates [12] by 3% - 13%, depending on the coating layers number.

For the value of spectral density $S^h_{\rm tech}$ of the other kinds of technical noise, we rely on the GWINC software tool [52].

### C. Optimization procedure

For each of the four configurations, of the two figures of merit described above, and of the two values of circulating power, $I_c = 200$ kW and $I_c = 840$ kW (16 variants in

total), we found maximums of the SNR integrals (2) and (4) over the parameter vector $\mathbf{p}$ and in the numbers of coating layers doublets of ITM, $N_{\rm ITM}$, and ETM, $N_{\rm ETM}$.

This optimization was performed in two steps. First, we maximised the SNRs in $\mathbf{p}$ for each of $N_{\rm ITM}$ and $N_{\rm ETM}$, using Nelder-Mead simplex method [53], and getting thus the semi-optimized values of SNR $\rho^2(N_{\rm ITM}, N_{\rm ETM})$ as a function of the numbers of coating layers doublets. At the second step, we found the optimal values of $N_{\rm ITM}$ and $N_{\rm ETM}$ by a simple grid search.

The following interferometer parameters were included into the parameter space of the vector $\mathbf{p}$ (depending on configuration):

$$\text{Plain: } \mathbf{p} = \{R_{\rm SRM}, \phi_{\rm SR}\}; \tag{6a}$$

$$\text{Squeezed: } \mathbf{p} = \{R_{\rm SRM}, \phi_{\rm SR}, e^r, \lambda\}; \tag{6b}$$

$$\text{Pre-filtering: } \mathbf{p} = \{R_{\rm SRM}, \phi_{\rm SR}, e^r, \lambda, \gamma_f, \delta_f\}; \tag{6c}$$

$$\text{Post-filtering: } \mathbf{p} = \{R_{\rm SRM}, \phi_{\rm SR}, \phi_{\rm LO}, e^r, \lambda, \gamma_f, \delta_f\}; \tag{6d}$$

where $R_{\rm SRM}$ is the signal recycling mirror power reflectivity, $\phi_{\rm SR}$ is the signal recycling cavity detuning angle, $\phi_{\rm LO}$ is the homodyne angle, $e^r$ is the squeezing factor and $\lambda$ is the squeezing angle, $\gamma_f$ is the filter cavity half-bandwidth and $\delta_f$ is the filter cavity detuning. For the reason discussed above, for all topologies except the post-filtering one, only two values of $\phi_{\rm SR}$ are considered: 0 (the extreme signal-recycling) and $\pi/2$ (the resonant-sideband-extraction).

We limited the squeezing factor by 10 dB ($e^r \le \sqrt{10}$), according to the contemporary experimental achievements in the low-frequency squeezing [54, 55].

The input laser power was limited by 500 W, which might seem unrealistically high. However, this value matches current plans for the Advanced LIGO enhancement with the proposed increase of the input laser power to 500−600 W [56], and also the plans to use a 1 kW laser in the future European third-generation gravitational-wave detector Einstein Telescope [57, 58].

In Fig. 2, we draw a typical relative SNR gain factor as a function of ITM and ETM number of coating layers doublets defined as follows:

$$G_{\rm rel}(N_{\rm ITM}, N_{\rm ETM}) = \frac{\rho^2(N_{\rm ITM}, N_{\rm ETM})}{\rho^2(N^{\rm def}_{\rm ITM}, N^{\rm def}_{\rm ETM})}\,, \tag{7}$$

where

$$N^{\rm def}_{\rm ITM} = 8\,, \qquad N^{\rm def}_{\rm ETM} = 19 \tag{8}$$

are the default values for the number of coating layers doublets prescribed by GWINC for the Advanced LIGO. Cyan dots correspond to $N_{\rm ITM} = N^{\rm def}_{\rm ITM}$, and the magenta ones — to $N_{\rm ETM} = N^{\rm def}_{\rm ETM}$. It is easy to see that for each $N_{\rm ITM}$, the optimal value of $N_{\rm ETM}$ exists, which corresponds to the balance of the quantum noise and the coating thermal noise. For smaller $N_{\rm ETM}$, the ETM transmittance is too big and the quantum noise dominates. Otherwise, the redundant number of the coating layers leads to a domination of the coating thermal noise.

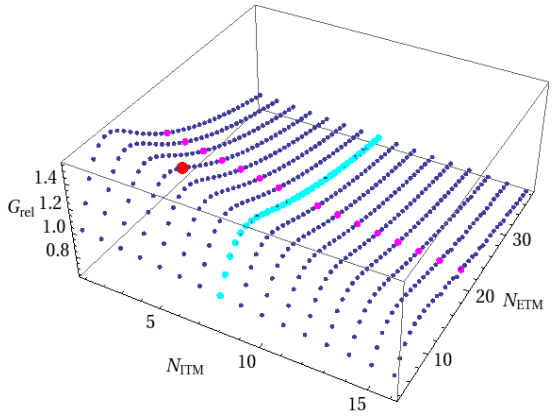


FIG. 2. Relative gain in SNR as a function of the coating layers doublets numbers $N_{\rm ITM}, N_{\rm ETM}$. Cyan and magenta dots correspond to the default numbers $N^{\rm def}_{\rm ITM} = 8$, $N^{\rm def}_{\rm ETM} = 19$ given by GWINC. Red dot marks the maximum signal-to-noise ratio given the technical limitations on the total power absorbed in the core optics discussed in Sec. II C.

At the same time, the dependence of $G_{\rm rel}(N_{\rm ITM}, N_{\rm ETM})$ on $N_{\rm ITM}$ displays no extremal behavior down to $N_{\rm ITM} = 0$. This means that our optimization algorithm tries to remove the noisy input mirrors completely, switching to the GEO-600 pure Michelson configuration [6], and providing the necessary bandwidth of the interferometer by means of the signal recycling mirror. Unfortunately, in fact, this regime can not be considered as the optimal one due to the following reasons. First, in our consideration, we have not taken into account the noise introduced by the beamsplitter. In a standard Fabry-Pérot/Michelson configuration with arm-cavity finesse $\mathcal{F} \gg 1$, the beamsplitter-induced noise can be neglected, as each reflection of the pump laser light from the beamsplitter corresponds to $\sim \mathcal{F}$ reflections inside the arm cavities, and thus it is suppressed by the factor $\sim \mathcal{F}^{-1}$. However, it becomes important if $N_{\rm ITM} \to 0$ and, therefore, $\mathcal{F} \to 1$. In particular, in the Advanced LIGO, the motion of the beamsplitter relative to the ETMs will be monitored by means of measurement of additional modulation sidebands of the carrier light resonant only in the power and signal recycling cavities, whereupon a sufficiently small value of $\mathcal{F}$ will imply much more stringent requirements on this monitoring system [59].

Second, for a given value of the circulating optical power in the arm cavities $I_c$, the power on the beamsplitter $I_{\rm BS}$ is proportional to $I_c\mathcal{F}^{-1}$, and very high power on the beamsplitter and ITMs can create undesirable effects like thermal lensing due to heating of the input mirrors and the beamsplitter by the absorbed optical power [60].

Due to these reasons, we limited the minimal number of the coating layers doublets on ITM by $N_{\rm ITM} = 4$, which corresponds to $\mathcal{F} \approx 20$. This value is sufficiently high to neglect with good precision the noise of the beamsplitter and to provide a reasonably low optical power on

the beamsplitter. In particular, in our estimates, we limited the power absorbed in each of the input mirrors and in the beamsplitter by 1 W. This value corresponds to a reasonably conservative order of magnitude estimate of the acceptable absorbed power [47] largely based on the current experimental experience in thermal lensing compensation. In principle, more deep optimization is possible which takes into account gradual degradation of the interferometer parameters with the increase of the absorbed power. However, in this optimization, many yet unknown factors have to be taken into account, *e.g.* novel thermal lensing compensation techniques. Therefore, such kind of optimization exceeds the scope of this paper.

A bold red dot in Fig. 2 corresponds to the optimal configuration conditional on the above mentioned constraints.

There are also other technical problems that may arise in the real interferometer. One of them is related to the pumping light leaving the arm cavities (that are usually impedance-matched for this light) through the ETMs. This light has a nonzero chance to return back into the cavities after scattering on the surrounding seismically not isolated objects and thus carrying random phase that may be a source of additional noise for the interferometer [61]. This scattering can be prevented by placing an absorbing plates with the power reflectivity $R_{\rm abs} \ll 1$ behind the ETMs. Simple estimate shows that in the case of a specular (mirror-like) reflection from these plates, the random motion thereof in a GW frequency band creates phase shifts of the light reflected back in the cavity mode of the order of $T_{\rm ETM}\sqrt{R_{\rm abs}} \sim 10^{-4}$ - $10^{-5}$ times smaller than that produced by the ETMs motion (assuming $R_{\rm abs} \approx 0.01$ and $T_{\rm ETM} \sim 10^{-3}$ - $10^{-4}$, see Tables IV, V). Note that in the double-mirror topology of [42], this factor is equal to just $T_{\rm ETM}$ that is at least one order of magnitude higher.

Another problem worth mentioning here is the increased bandwidth of the interferometer common mode (created by the arm cavities and the power recycling mirror) due to reduced finesse of the arm cavities. In the DC readout configuration, it leads to proportionally increased fluctuations of the local oscillator light [62]. However, for the parameters which we use for estimates here, this effect is compensated partly due to increased reflectivity of the power recycling mirror. As a result, the common mode bandwidth increases about twofold in the case of 840 kW of circulating power, and by about one order of magnitude in the case of 200 kW of circulating power. Taking into account that the local oscillator noise is not considered as one of the main sensitivity limiting factors for the aLIGO, the overall sensitivity should not be significantly affected by this effect.

## III. DISCUSSION

The results of the optimization are given in Tables II and III for the BNS and burst sources, respectively. In addition, the explicit values of the optimized vectors **p** are shown in Tables IV and V in the Appendix.

It follows from these results, that reducing $N_{\rm ITM}$ from $N_{\rm ITM}^{\rm def} = 8$ to 4, and $N_{\rm ETM}$ from $N_{\rm ETM}^{\rm def} = 19$ to 14 for $I_c = 840\,{\rm kW}$ and to 11-12 for $200\,{\rm kW}$, it is possible to increase the signal to noise ratio $\rho^2$ for the BNS events by $\sim 20$ - $30\%$, or for the burst events — by $\sim 15$ - $20\%$, depending on the interferometer topology, see the corresponding columns labeled "$G_{\rm rel}$".

We are also able to compare the performance of the interferometers which employ different advanced techniques like squeezing, pre- and post-filtering with the baseline design, characterized by

$$I_c = 840\,{\rm kW}\,, \quad r = 0\,, \quad N_{\rm ITM}^{\rm def} = 8\,, \quad N_{\rm ETM}^{\rm def} = 19\,. \quad (9)$$

For this purpose, we introduce an absolute gain defined as:

$$G_{\rm abs} = \frac{\rho^2}{\rho^2_{\rm base}}\,, \quad (10)$$

with $\rho^2_{\rm base}$ related to the *baseline* interferometer. The corresponding values of $G_{\rm abs}$ are given in Tables II and III.

These numbers tell us that for the GW bursts, the near-four-fold increase of the circulating power results in the about two-fold relative rise of the SNR, yet almost the same result can be achieved by employing a 10 dB input squeezing. At the same time, the BNS signal-to-noise ratio $\rho^2_{\rm BNS}$ scales much more weakly with the power increase, and does not benefit significantly from the squeezing (note that in this case, the optimization algorithm recommends only moderate values of $r$ for the frequency-independent squeezing).

The physics behind such a behavior is transparent. For the sensitivity of the detector to GW bursts depend on the high frequency shot-noise-dominated part of the noise budget (inversely proportional to the product of circulating power $I_c$ and squeezing factor $e^{2r}$) to a greater extent ($h_{\rm burst}(\Omega) \propto \Omega^{-1/2}$) compared to the sensitivity to gravitational waves emitted by compact binary systems ($h_{\rm BNS}(\Omega) \propto \Omega^{-7/6}$), the former one displays the expected trend described above. At the same time, BNS sensitivity assigns more weight to the radiation-pressure-dominated low-frequency region and to medium frequencies equally sensitive to both parts of quantum noise, thus making it much harder to balance their influence, for the radiation pressure fluctuations have opposite dependence on power and squeezing factor as the shot noise.

Another apparent conclusion yielding from our optimization is that even a relatively short ($l = 50$ m) filter cavity, providing that sufficiently good mirrors are available (losses per bounce $A_f = 10\,{\rm ppm}$ are considered as a viable option for post-Advanced LIGO detectors filter

TABLE II. BNS optimization.

| Configuration | $I_c\,[kW]$ | $N_{ITM}$ | $N_{ETM}$ | $I_0$ [kW] | $I_{\rm BS}$ [kW] | $e^{2r}$ | $G_{\rm rel}$ | $G_{\rm abs}$ |
|---|---|---|---|---|---|---|---|---|
| Plain (DC-readout) | 200 | 4 | 11 | 0.50 | 16 | – | 1.18 | 1.03 |
| Squeezed (DC-readout) | 200 | 4 | 11 | 0.50 | 16 | 3.2 | 1.24 | 1.25 |
| Pre-filtering (DC-readout) | 200 | 4 | 11 | 0.50 | 16 | 10 | 1.32 | 2.43 |
| Post-filtering (Homodyne) | 200 | 4 | 12 | 0.26 | 16 | 8.6 | 1.33 | 2.39 |
| Plain (DC-readout) | 840 | 4 | 14 | 0.39 | 68 | – | 1.17 | |
| Squeezed (DC-readout) | 840 | 4 | 14 | 0.39 | 68 | 2.7 | 1.22 | 1.35 |
| Pre-filtering (DC-readout) | 840 | 4 | 14 | 0.39 | 68 | 10 | 1.30 | 2.65 |
| Post-filtering (Homodyne) | 840 | 4 | 14 | 0.39 | 68 | 10 | 1.30 | 2.65 |

TABLE III. Bursts optimization.

| Configuration | $I_c\,[kW]$ | $N_{ITM}$ | $N_{ETM}$ | $I_0$ [kW] | $I_{\rm BS}$ [kW] | $e^{2r}$ | $G_{\rm rel}$ | $G_{\rm abs}$ |
|---|---|---|---|---|---|---|---|---|
| Plain (DC-readout) | 200 | 4 | 11 | 0.50 | 16 | – | 1.14 | 0.52 |
| Squeezed (DC-readout) | 200 | 4 | 12 | 0.26 | 16 | 10 | 1.15 | 1.26 |
| Pre-filtering (DC-readout) | 200 | 4 | 12 | 0.26 | 16 | 10 | 1.21 | 1.50 |
| Post-filtering (Homodyne) | 200 | 4 | 12 | 0.26 | 16 | 10 | 1.22 | 1.52 |
| Plain (DC-readout) | 840 | 4 | 14 | 0.39 | 68 | – | 1.14 | |
| Squeezed (DC-readout) | 840 | 4 | 14 | 0.39 | 68 | 10 | 1.16 | 2.71 |
| Pre-filtering (DC-readout) | 840 | 4 | 14 | 0.39 | 68 | 10 | 1.21 | 3.10 |
| Post-filtering (Homodyne) | 840 | 4 | 14 | 0.39 | 68 | 10 | 1.21 | 3.12 |

cavities) [36], is capable of quite significant sensitivity gain for both considered GW sources.

It is interesting to note that for all considered topologies, the optimization algorithm gives very small values of the signal recycling mirror reflectivity $R_{SRM} \ll 1$, actually rejecting the signal recycling completely, see Tables IV and V. The reason for this is evident: the reduced number of coating layers in input mirrors gives increases the arm cavities bandwidth, making it close to the optimal one for the broadband gravitational-wave signals without the signal recycling mirror assistance.

Plots of the optimal spectral densities for both quantum and technical noise are drawn in Figs. 3 and 4 for BNS and GW bursts, respectively. We elected for plotting only the most promising variants with fixed and frequency-dependent input squeezing. For comparison, the corresponding spectral densities for the default numbers of the coating layers doublets (8), as well as for the "baseline" configuration (9) are shown there as well. These plots demonstrate that the optimization procedure considered here, while suppressing noticeably the sum technical noise, introduces only minor changes into the quantum noise. The only exception is the BNS optimization in the absence of the filter cavity, which reduces the quantum noise in the best sensitivity area around 100 Hz, following the technical noise, at the price of narrower width of this region.

We would like to emphasize that our solution to the coating thermal noise problem provides a 20-30% gain in the signal-to-noise ratio for the two most probable astrophysical sources of GWs which amounts in the 30-50% increase of the event rate without any significant change to the optical layout of the GW interferometer. The price one has to pay, namely about two-fold increase of the input laser power, slightly higher absorbed power in the core optics and other issues mentioned above, can not be considered as a prohibitive one for this sensitivity gain.

The above consideration shows that if it were not for the high optical power, typical for the large-scale GW detectors, and the ensuing discussed limitations on the core optics, the sensitivity gain would be much higher. However, for shorter baseline interferometers like the Hannover 10-meter prototype [43], significantly higher gain is possible due to much lower optical power required for its operation.

## ACKNOWLEDGMENTS

The authors are very grateful to Matt Evans for going to the trouble of thorough reading the manuscript and, especially, for his critical remarks that were very illuminating and useful for improving the quality of this article.

This work was supported by the Russian Foundation for Basic Research Grant No. 08-02-00580-a. The work of F.Ya.Khalili was supported by NSF and Caltech Grant No. PHY-0967049. Stefan Danilishin was supported by the David and Barbara Groce Startup Fund at the California Institute of Technology via the CRDF Grant

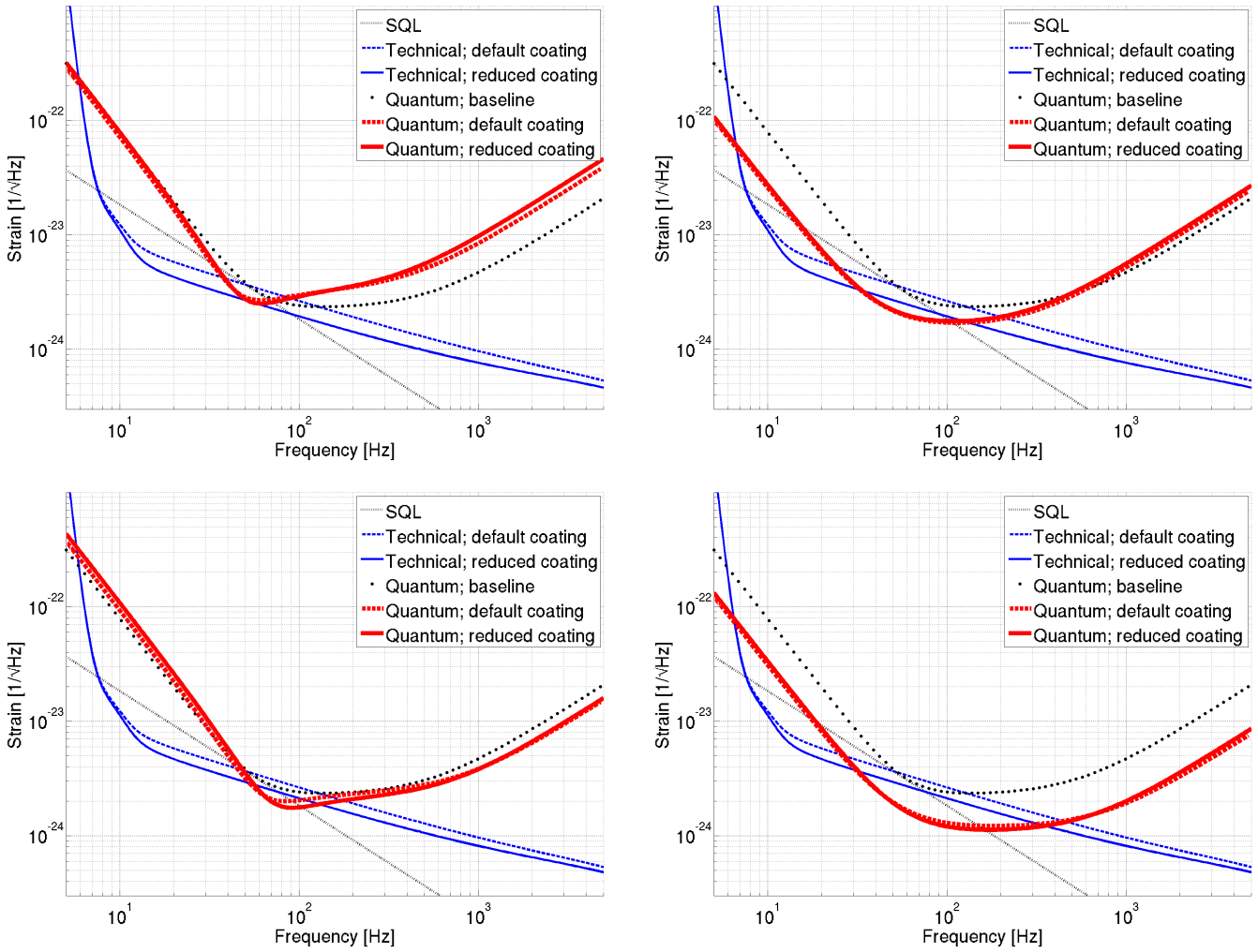


FIG. 3. Optimal quantum and technical noise spectral densities for the BNS sources. Left column: schemes with frequency-independent squeezing (referred to as "squeezed"); right column: schemes with frequency-dependent input squeezing (referred to as "pre-filtering"). Top row: $I_c = 200\,\mathrm{kW}$, bottom row: $I_c = 840\,\mathrm{kW}$. Solid lines: optimized numbers of the coating layer doublets $N_{\mathrm{ITM}}$ and $N_{\mathrm{ETM}}$; dashed lines: default numbers $N_{\mathrm{ITM}} = 8$ and $N_{\mathrm{ETM}} = 19$. Dash-dotted line: "baseline" configuration: $I_c = 840\,\mathrm{kW}$, $N_{\mathrm{ITM}} = 8$ and $N_{\mathrm{ETM}} = 19$, no squeezing; dotted line: SQL.

RUP1-32011-MO-10.

The paper has been assigned LIGO document number P1100199.

## Appendix: Quantum noise spectral densities

### 1. Notations

We base our consideration here on the Caves-Schumaker's two-photon formalism [63, 64]. Treatment of all of the considered schemes of the interferometers is done is accordance with [65] where all the detailed derivations can be found. Two-photon quadrature vectors are denoted by boldface letters, and their components — by upright letters, *e.g.*

$$\hat{\mathbf{a}} = \begin{pmatrix} \hat{\mathrm{a}}_1 \\ \hat{\mathrm{a}}_2 \end{pmatrix}. \tag{A.1}$$

$2 \times 2$ matrices are denoted by "blackboard bold" letters, *e.g.* $\mathbb{R}$.

The quadrature amplitudes are normalized in such a way, that in the vacuum quantum state, their single-sided spectral densities are equal to one, *e.g.*

$$S[\hat{\mathrm{g}}_1] = S[\hat{\mathrm{g}}_2] = 1\,. \tag{A.2}$$

We use the following notation for the norms of the two-components quadrature vectors:

$$\forall \mathbf{A} = \begin{pmatrix} A_1 \\ A_2 \end{pmatrix} : \quad \|\mathbf{A}\|^2 = \mathbf{A}^{\mathsf{T}}\mathbf{A}\,. \tag{A.3}$$

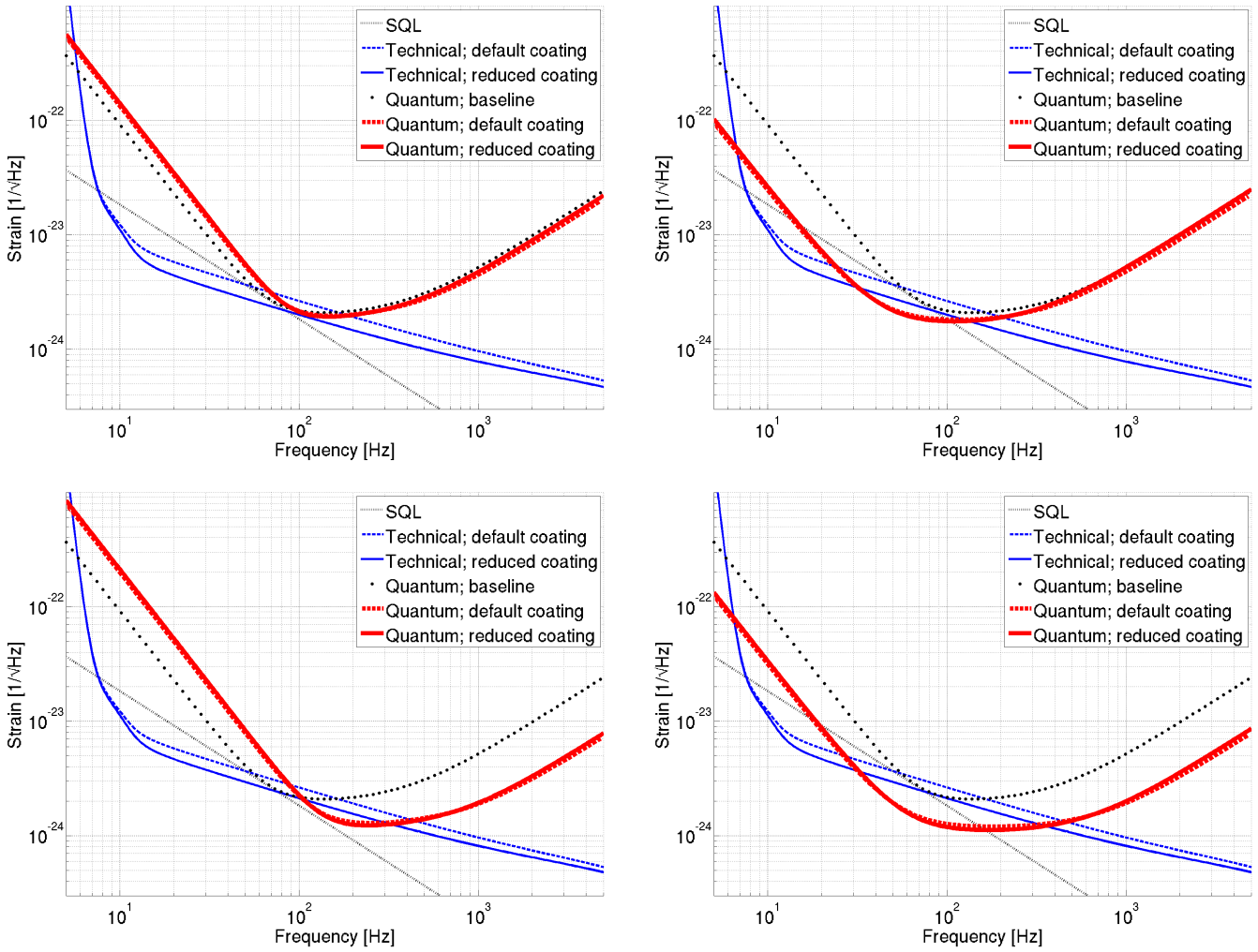


FIG. 4. Optimal quantum and technical noise spectral densities for the burst sources. Left column: schemes with frequency-independent squeezing (referred to as "squeezed"); right column: schemes with frequency-dependent input squeezing (referred to as "pre-filtering"). Top row: $I_c = 200\,\mathrm{kW}$, bottom row: $I_c = 840\,\mathrm{kW}$. Solid lines: optimized numbers of the coating layer doublets $N_{\mathrm{ITM}}$ and $N_{\mathrm{ETM}}$; dashed lines: default numbers $N_{\mathrm{ITM}} = 8$ and $N_{\mathrm{ETM}} = 19$. Dash-dotted line: "baseline" configuration, see Eq. (9); dotted line: SQL.

### 2. Input-output relations

#### a. *Michelson/Fabry-Pérot interferometer*

Following the treatment of paper [51] (often referred to as "scaling law"), the Fourier-domain input/output relations of a signal-recycled Michelson/Fabry-Pérot interferometer detector can be written in the equivalent form of the single effective Fabry-Pérot cavity input/output relations:

$$\hat{\mathbf{b}}(\Omega) = \mathbb{R}(\Omega)\hat{\mathbf{a}}(\Omega) + \mathbb{T}(\Omega)\hat{\mathbf{g}}(\Omega) + \mathbf{R}(\Omega)\chi(\Omega)\frac{G(\Omega)}{2}. \quad \text{(A.4)}$$

Here $\hat{\mathbf{a}}$, $\hat{\mathbf{b}}$, $\hat{\mathbf{g}}$ are the quadrature vectors of, respectively, the input light, the output light and the vacuum noise which arises due to the optical losses in the interferometer,

$$\mathbb{R}(\Omega) = \frac{1}{\mathcal{D}(\Omega) - J\delta/\Omega^2}\begin{pmatrix} R_{11} & R_{12} \\ R_{21} & R_{22}\end{pmatrix}, \quad \text{(A.5a)}$$

$$R_{11} = R_{22} = 2\gamma_1(\gamma - \mathrm{i}\Omega) - \mathcal{D}(\Omega) + J\delta/\Omega^2\,,$$
$$R_{12} = -2\gamma_1\delta\,, \quad R_{21} = 2\gamma_1\delta - 2J\gamma_1/\Omega^2\,,$$

$$\mathbb{T}(\Omega) = \frac{2\sqrt{\gamma_1\gamma_2}}{\mathcal{D}(\Omega) - J\delta/\Omega^2}\begin{pmatrix} \gamma - \mathrm{i}\Omega & -\delta \\ \delta - J/\Omega^2 & \gamma - \mathrm{i}\Omega\end{pmatrix}, \quad \text{(A.5b)}$$

$$\mathcal{D}(\Omega) = (\gamma - i\Omega)^2 + \delta^2\,, \quad J = \frac{8\omega_p I_c}{McL}\,, \quad \text{(A.6)}$$

$$\delta = \frac{2\sqrt{R_{\rm SRM}}\sin(2\phi_{\rm SR})\gamma_{\rm ITM}}{1+2\sqrt{R_{\rm SRM}}\cos(2\phi_{\rm SR})+R_{\rm SRM}}\,, \tag{A.7a}$$

$$\gamma_1 = \frac{(1-R_{\rm SRM})\,\gamma_{\rm ITM}}{1+2\sqrt{R_{\rm SRM}}\cos(2\phi_{\rm SR})+R_{\rm SRM}}\,, \tag{A.7b}$$

$$\gamma = \gamma_1 + \gamma_2\,, \tag{A.7c}$$

$$\gamma_{\rm ITM} = \frac{c\,T_{\rm ITM}}{4L}, \quad \gamma_2 = \gamma_{\rm ETM} = \frac{cT_{\rm ETM}}{4L}\,, \tag{A.7d}$$

$T_{\rm ITM}$ is the power transmissivity of the ITMs, $T_{\rm ETM}$ is the ETMs transmissivity accumulating all the optical losses in the interferometer, $R_{\rm SRM} = 1 - T_{\rm SRM}$ is the power reflectivity of SRM, and $\phi_{\rm SR} = \omega_p l_{\rm SR}/c$ is the single trip detuning phase of the carrier light in the SR-cavity with length $l_{\rm SR}$.

Vector

$$\mathbf{R}(\Omega) = \sqrt{\frac{2\gamma_1 JM}{\hbar}}\frac{1}{\mathcal{D}(\Omega)}\begin{pmatrix}-\delta\\ \gamma - \mathrm{i}\Omega\end{pmatrix}, \tag{A.8}$$

stands for the interferometer optical response function to the differential mechanical motion of the test masses (dARM mode) induced by the GW tidal force:

$$G(\Omega) = -ML\Omega^2 h(\Omega) \tag{A.9}$$

acting on the ETMs, and

$$\chi(\Omega) = \frac{1}{-M\Omega^2 + K(\Omega)} \tag{A.10}$$

is the mechanical susceptibility of the dARM mode modified by the optical rigidity

$$K(\Omega) = \frac{MJ\delta}{\mathcal{D}(\Omega)}. \tag{A.11}$$

#### b. *Filter cavity*

The input/output relations for the filter cavity have the following form:

$$\hat{\mathbf{o}}(\Omega) = \mathbb{R}_f(\Omega)\hat{\mathbf{i}}(\Omega) + \mathbb{T}_f(\Omega)\hat{\mathbf{q}}(\Omega), \tag{A.12}$$

with $\hat{\mathbf{i}}$, $\hat{\mathbf{o}}$, and $\hat{\mathbf{q}}$ being the two-photon quadratures vectors of, respectively, the input, output and additional vacuum, induced by the optical losses in the filter cavity, quantum fields that fully describe all the filter cavity inputs and outputs, and

$$\mathbb{R}_f(\Omega) = \frac{1}{\mathcal{D}_f(\Omega)}\begin{pmatrix}R_{f11} & R_{f12}\\ R_{f21} & R_{f22}\end{pmatrix}, \tag{A.13a}$$

$$R_{f11} = R_{f22} = \gamma_{f1}^2 - \gamma_{f2}^2 - \delta_f^2 + \Omega^2 + 2\mathrm{i}\Omega\gamma_{f2},$$
$$R_{f12} = -R_{f21} = -2\gamma_{f1}\delta_f,$$

$$\mathbb{T}_f(\Omega) = \frac{2\sqrt{\gamma_{f1}\gamma_{f2}}}{\mathcal{D}_f(\Omega)}\begin{pmatrix}\gamma_f - \mathrm{i}\Omega & -\delta_f\\ \delta_f & \gamma_f - \mathrm{i}\Omega\end{pmatrix}, \tag{A.13b}$$

$$\mathcal{D}_f(\Omega) = (\gamma_f - i\Omega)^2 + \delta_f^2\,, \tag{A.14}$$

$\delta_f$ is the filter cavity detuning, $\gamma_f = \gamma_{f1} + \gamma_{f2}$ is its half-bandwidth,

$$\gamma_{f1} = \frac{c\,T_f}{4L_f}, \quad \gamma_{f2} = \frac{c\,A_f}{4L_f}, \tag{A.15}$$

$T_f$ is the power transmissivity of the input/output mirror of filter cavity with length $L_f$, and $A_f$ is the coefficient of optical power losses per bounce.

#### c. *Detector*

We model the DC readout detector as a homodyne detector with a fixed local oscillator phase equal to $\pi/2$.

The detector quantum efficiency $\eta < 1$ is modeled by an imaginary gray filter with a power transmissivity $\eta$:

$$\hat{\mathbf{d}}' = \sqrt{\eta}\,\hat{\mathbf{d}} + \sqrt{1-\eta}\,\hat{\mathbf{n}}\,, \tag{A.16}$$

where $\hat{\mathbf{d}}$ is the quadrature vector of the photodetector incident field, $\hat{\mathbf{d}}'$ is the effective incoming field, and $\hat{\mathbf{n}}$ is the additional vacuum noise associated with the the photodetector quantum inefficiency $1-\eta$.

The output signal of the homodyne detector (the photocurrent) is proportional to

$$i(\Omega) \propto \mathbf{H}^{\mathsf{T}}\hat{\mathbf{d}}'(\Omega) \propto \mathbf{H}^{\mathsf{T}}\big[\hat{\mathbf{d}}(\Omega) + \epsilon_d\hat{\mathbf{n}}(\Omega)\big], \tag{A.17}$$

where

$$\epsilon_d = \sqrt{\frac{1}{\eta} - 1} \tag{A.18}$$

and

$$\mathbf{H} = \begin{pmatrix}\cos\phi_{\rm LO}\\ \sin\phi_{\rm LO}\end{pmatrix} \tag{A.19}$$

is the homodyne vector.

### 3. Configurations

#### a. *"Plain" interferometer*

In this case,

$$\hat{\mathbf{d}} = \hat{\mathbf{b}}\,, \tag{A.20}$$

and the incoming field $\hat{\mathbf{a}}$ is in the vacuum quantum state.

Combination of Eqs. (A.4, A.20, A.16) gives the following single-sided spectral density of the quantum noise in the units of gravitational-wave strain $h$:

$$S^h_{\rm plain}(\Omega) = \frac{8}{M^2L^2\Omega^4} \times \frac{\|\mathbb{R}^\dagger(\Omega)\mathbf{H}\|^2 + \|\mathbb{T}^\dagger(\Omega)\mathbf{H}\|^2 + \epsilon_d^2}{\left|\mathbf{H}^{\mathsf{T}}\mathbf{R}(\Omega)\chi(\Omega)\right|^2}\,. \tag{A.21}$$

*b. Squeezed input*

In this case, the incident field $\hat{\mathbf{a}}$ is the result of squeezing of some vacuum filed $\hat{\mathbf{z}}$:

$$\hat{\mathbf{a}}(\Omega) = \mathbb{S}\hat{\mathbf{z}}(\Omega)\,, \tag{A.22}$$

with squeezing matrix defined as:

$$\mathbb{S} = \begin{pmatrix} \cosh r + \cos 2\lambda \sinh r & \sin 2\lambda \sinh r \\ \sin 2\lambda \sinh r & \cosh r - \cos 2\lambda \sinh r \end{pmatrix}. \tag{A.23}$$

Combining Eq. (A.22) with Eqs. (A.4, A.20, A.16), we obtain:

$$S^h_{\rm sqz}(\Omega) = \frac{8}{M^2L^2\Omega^4} \times \frac{\|\mathbb{S}\mathbb{R}^\dagger(\Omega)\mathbf{H}\|^2 + \|\mathbb{T}^\dagger(\Omega)\mathbf{H}\|^2 + \epsilon_d^2}{\left|\mathbf{H}^\mathsf{T}\mathbf{R}(\Omega)\chi(\Omega)\right|^2}\,. \tag{A.24}$$

*c. Pre-filtering*

In the pre-filtering scheme, the incident field with frequency-dependent squeezing angle $\lambda(\Omega)$ is created by means of passing the squeezed light with frequency-independent squeezing (A.22) through the filter cavity, see Eq. (A.12):

$$\hat{\mathbf{a}}(\Omega) = \mathbb{R}_f(\Omega)\mathbb{S}\hat{\mathbf{z}}(\Omega) + \mathbb{T}_f(\Omega)\hat{\mathbf{q}}(\Omega)\,. \tag{A.25}$$

Combining Eq. (A.25) with (A.4, A.20, A.16), we obtain:

$$S^h_{\rm pre}(\Omega) = \frac{8}{M^2L^2\Omega^4} \times \frac{1}{\left|\mathbf{H}^\mathsf{T}\mathbf{R}(\Omega)\chi(\Omega)\right|^2} \times \Big[\|\mathbb{S}\mathbb{R}_f^\dagger(\Omega)\mathbb{R}^\dagger(\Omega)\mathbf{H}\|^2 + \|\mathbb{T}_f^\dagger(\Omega)\mathbb{R}^\dagger(\Omega)\mathbf{H}\|^2 + \|\mathbb{T}^\dagger(\Omega)\mathbf{H}\|^2 + \epsilon_d^2\Big]. \tag{A.26}$$

*d. Post-filtering*

In the post-filtering scheme, the outgoing field of the interferometer passes though the filter cavity:

$$\hat{\mathbf{d}}(\Omega) = \mathbb{R}_f(\Omega)\mathbb{S}\hat{\mathbf{b}}(\Omega) + \mathbb{T}_f(\Omega)\hat{\mathbf{q}}(\Omega)\,. \tag{A.27}$$

The chain of Eqs. (A.22, A.4, A.27, A.16) gives the following spectral density:

$$S^h_{\rm post}(\Omega) = \frac{8}{M^2L^2\Omega^4} \times \frac{1}{\left|\mathbf{H}^\mathsf{T}\mathbb{R}_f(\Omega)\mathbf{R}(\Omega)\chi(\Omega)\right|^2} \times \Big[\|\mathbb{S}\mathbb{R}^\dagger(\Omega)\mathbb{R}_f^\dagger(\Omega)\mathbf{H}\|^2 + \|\mathbb{T}^\dagger(\Omega)\mathbb{R}_f^\dagger(\Omega)\mathbf{H}\|^2 + \|\mathbb{T}_f^\dagger(\Omega)\mathbf{H}\|^2 + \epsilon_d^2\Big]. \tag{A.28}$$

TABLE IV. BNS optimization.

| Configuration | $I_c$ [$kW$] | $T_{ITM}$ | $T_{ETM}$ | $R_{SRM}$ | $\phi_{SRC}$ [rad] | $\phi_{LO}$ [rad] | $\lambda$ [rad] | $e^{2r}$ | $\gamma_I$ [Hz] | $\delta_f$ [Hz] |
|---|---|---|---|---|---|---|---|---|---|---|
| Plain (DC-readout) | 200 | 0.15 | $1 \cdot 10^{-3}$ | 0.10 | 0 | $\pi/2$ | – | – | – | – |
| Squeezed (DC-readout) | 200 | 0.15 | $1 \cdot 10^{-3}$ | 0.02 | 0 | $\pi/2$ | 0.38 | 3.2 | – | – |
| Pre-filtering (DC-readout) | 200 | 0.15 | $1 \cdot 10^{-3}$ | 0.06 | 0 | $\pi/2$ | -0.03 | 10 | 194 | 194 |
| Post-filtering (Homodyne) | 200 | 0.15 | $6 \cdot 10^{-4}$ | 0.10 | -0.21 | 1.82 | 0.68 | 8.6 | 156 | 220 |
| Plain (DC-readout) | 840 | 0.15 | $1 \cdot 10^{-4}$ | 0.00 | $\pi/2$ | $\pi/2$ | – | – | – | – |
| Squeezed (DC-readout) | 840 | 0.15 | $1 \cdot 10^{-4}$ | 0.04 | $\pi/2$ | $\pi/2$ | 0.38 | 2.7 | – | – |
| Pre-filtering (DC-readout) | 840 | 0.15 | $1 \cdot 10^{-4}$ | 0.02 | $\pi/2$ | $\pi/2$ | -0.02 | 10 | 262 | 262 |
| Post-filtering (Homodyne) | 840 | 0.15 | $1 \cdot 10^{-4}$ | 0.06 | -1.17 | 1.77 | 0.83 | 10 | 190 | 264 |

TABLE V. Bursts optimization.

| Configuration | $I_c$ [$kW$] | $T_{ITM}$ | $T_{ETM}$ | $R_{SRM}$ | $\phi_{SRC}$ [rad] | $\phi_{LO}$ [rad] | $\lambda$ [rad] | $e^{2r}$ | $\gamma_I$ [Hz] | $\delta_f$ [Hz] |
|---|---|---|---|---|---|---|---|---|---|---|
| Plain (DC-readout) | 200 | 0.15 | $1 \cdot 10^{-3}$ | 0.16 | 0 | $\pi/2$ | – | – | – | – |
| Squeezed (DC-readout) | 200 | 0.15 | $6 \cdot 10^{-4}$ | 0.00 | 0 | $\pi/2$ | 0.03 | 10 | – | – |
| Pre-filtering (DC-readout) | 200 | 0.15 | $6 \cdot 10^{-4}$ | 0.04 | 0 | $\pi/2$ | -0.01 | 10 | 172 | 174 |
| Post-filtering (Homodyne) | 200 | 0.15 | $6 \cdot 10^{-4}$ | 0.03 | 0.00 | 1.62 | 0.04 | 10 | 173 | 176 |
| Plain (DC-readout) | 840 | 0.15 | $1 \cdot 10^{-4}$ | 0.01 | 0 | $\pi/2$ | – | – | – | – |
| Squeezed (DC-readout) | 840 | 0.15 | $1 \cdot 10^{-4}$ | 0.06 | $\pi/2$ | $\pi/2$ | 0.02 | 10 | – | – |
| Pre-filtering (DC-readout) | 840 | 0.15 | $1 \cdot 10^{-4}$ | 0.02 | $\pi/2$ | $\pi/2$ | 0.00 | 10 | 253 | 253 |
| Post-filtering (Homodyne) | 840 | 0.15 | $1 \cdot 10^{-4}$ | 0.02 | -1.56 | 1.60 | 0.03 | 10 | 260 | 265 |

[1] http://www.ligo.caltech.edu.
[2] S.J.Waldman (for the LIGO Science Collaboration), Classical and Quantum Gravity **23**, S653 (2006).
[3] http://www.virgo.infn.it/.
[4] F.Acernese *et al*, Classical and Quantum Gravity **23**, S635 (2006).
[5] http://geo600.aei.mpg.de.
[6] S.Hild (for the LIGO Scientific Collaboration), Classical and Quantum Gravity **23**, S643 (2006).
[7] http://tamago.mtk.nao.ac.jp.
[8] M.Ando and the TAMA Collaboration, Classical and Quantum Gravity **22**, S881 (2005).
[9] C.M.Caves, Physical Review D **23**, 1693 (1981).
[10] B. Mours, E. Tournefier, and J.-Y. Vinet, Classical and Quantum Gravity **23**, S777 (2006).
[11] M. Bondarescu and K.S. Thorne, Physical Review D **74**, 082003 (2006).
[12] G. M. Harry et al., Classical and Quantum Gravity **24**, 405 (2007).
[13] H.J.Kimble, and B.L.Lev, and J.Ye, Phys. Rev. Lett. **101**, 260602 (2008).
[14] M. Bondarescu, O. Kogan, and Y. Chen, Phys. Rev. D **78**, 082002 (2008).
[15] A. E. Villar et al., Physical Review D **81**, 122001 (2010).
[16] T. Hong, J. Miller, H. Yamamoto, Y. Chen, and R. Adhikari, Physical Review D **84** 102001 (2011).
[17] N. M. Kondratiev, A. G. Gurkovsky, and M. L. Gorodetsky, Phys. Rev. D **84**, 022001 (2011).
[18] G. Harry, T. Bodiya, and R. Desalvo, editors, *Optical Coatings for Precision Measurement*, Cambridge University Press, in press.
[19] W.G.Unruh, in *Quantum Optics, Experimental Gravitation, and Measurement Theory*, edited by P.Meystre and M.O.Scully, page 647, Plenum Press, New York, 1982.
[20] V. B. Braginsky, F. Ya. Khalili, Physics Letters A **147**, 251 (1990).
[21] V.B.Braginsky, F.Ya.Khalili, Physics Letters A **257**, 241 (1999).
[22] A.Buonanno, Y.Chen, Physical Review D **64**, 042006 (2001).
[23] F.Ya.Khalili, Physics Letters A **288**, 251 (2001).
[24] A.Buonanno, Y.Chen, Physical Review D **65**, 042001 (2002).
[25] H.J.Kimble, Yu.Levin, A.B.Matsko, K.S.Thorne and S.P.Vyatchanin, Physical Review D **65**, 022002 (2001).
[26] Y.Chen, Physical Review D **67**, 122004 (2003).
[27] Thomas Corbitt, Nergis Mavalvala, and Stan Whitcomb, Physical Review D **70**, 022002 (2004).
[28] S.L.Danilishin, Physical Review D **69**, 102003 (2004).
[29] H.Rehbein, H.Muller-Ebhardt, K.Somiya, S.L.Danilishin, R.Schnabel, K.Danzmann, Y.Chen, Physical Review D **78**, 062003 (2008).
[30] I.S. Kondrashov, D.A. Simakov, F.Ya. Khalili and S.L. Danilishin, Physical Review D **78**, 062004 (2008).
[31] F.Ya.Khalili, H.Miao, and Y.Chen, Physical Review D **80**, 042006 (2009).
[32] Y.Chen, S.L.Danilishin, F.Y.Khalili, H.Müller-Ebhardt, General Relativity and Gravitation **43**, 671 (2011).
[33] F. Khalili et al., Phys. Rev. D **83**, 062003 (2011).
[34] www.advancedligo.mit.edu.
[35] G.M.Harry (for the LIGO Scientic Collaboration), Classical and Quantum Gravity **27**, 084006 (2010).
[36] *Instrument Science White Paper*, LIGO Scientific Collaboration, LIGO document T1200199 (2012).
[37] http://wwwcascina.virgo.infn.it/advirgo/.
[38] http://www.icrr.u-tokyo.ac.jp/gr/LCGT.html.
[39] J.Abadie *et al*, Nature Physics , Published online 11 September (2011).
[40] G. M. Harry et al., Appl. Opt. **45**, 1569 (2006).
[41] V.B.Braginsky, S.P.Vyatchanin, Physics Letters A **324**, 345 (2004).
[42] F.Ya.Khalili, Physics Letters A **334**, 67 (2005).
[43] S.Gossler and *et al*, Classical and Quantum Gravity **27**, 084023 (2010).
[44] F. Y. Khalili, Phys. Rev. D **83**, 122001 (2011).
[45] S.P.Tarabrin, Diffractional losses in corner reflectors, in *Proceedings of 7th International Conference on Laser and Fiber-Optical Networks Modeling*, pages 240–243, 2005.
[46] S.Gossler, *private communication.*
[47] Rana Adhikari, *private communication.*
[48] F.Ya.Khalili, Physical Review D **81**, 122002 (2010).
[49] F.Ya.Khalili, Physical Review D **77**, 062003 (2008).
[50] K.A.Postnov, L.R.Yungelson, Living Reviews in Relativity **9** (2006).
[51] A.Buonanno, Y.Chen, Physical Review D **67**, 062002 (2003).
[52] Gravitational Wave Interferometer Noise Calculator (GWINC), https://nodus.ligo.caltech.edu:30889/wiki/doku.php?id=aic_wiki.
[53] GNU scientific library, http://www.gnu.org/s/gsl.
[54] H. Vahlbruch et al., Phys. Rev. Lett. **100**, 033602 (2008).
[55] M.Mehmet *et al*, arXiv:1110.3737 (2011).
[56] LIGO *Instrument Science White Paper*, 2012.
[57] M.Punturo *et al*, Classical and Quantum Gravity **27**, 084007 (2010).
[58] S. Hild *et al*, Classical and Quantum Gravity **28**, 094013 (2011).
[59] R.Abbot *et al*, Advanced ligo length sensing and control final design, 2010, LIGO document T1000298-T.
[60] Patrice Hello and Jean-Yves Vinet, J. Phys. France **51**, 1267-1282 (1990).
[61] Matt Evans, *private communication.*
[62] Tobin T. Fricke *et al*, Classical and Quantum Gravity **29**, 065005 (2012).
[63] C.M.Caves and B.L.Schumaker, Physical Review A **31**, 3068 (1985).
[64] B.L.Schumaker and C.M.Caves, Physical Review A **31**, 3093 (1985).
[65] S.L.Danilishin, F.Ya.Khalili, Quantum measurement theory in gravitational-wave detectors, accepted for publication in *Living Reviews in Relativity*, 2012.